Optical spin resonance and transverse spin relaxation in magnetic semiconductor quantum wells

S. A. Crooker and D. D. Awschalom
Department of Physics, University of California, Santa Barbara, California 93106

J. J. Baumberg
Hitachi Cambridge Laboratory, Madingley Road, Cambridge CB3 0HE, United Kingdom

F. Flack and N. Samarth
Department of Physics, Pennsylvania State University, University Park, Pennsylvania 16802
(Received 2 April 1997)

Ultrafast optical pulses are used to initiate and measure free-induction decays of coherent conduction electron spins and of embedded magnetic Mn^{2+} ions in a series of magnetic-semiconductor quantum wells. These time-resolved Faraday rotation experiments in transverse applied magnetic fields complement previous studies of spin dynamics in longitudinal fields by unambiguously distinguishing between the spin relaxation of electrons and holes, and by identifying a mechanism by which angular momentum is transferred from spin-polarized carriers to the sublattice of local moments. In transverse fields (Voigt geometry), the precession of the photoexcited spins about the field axis can be measured as an oscillatory induced Faraday rotation signal. We observe the THz free-induction decay of spin-polarized electrons in modest (<4 T) magnetic fields and separately identify the more rapid spin relaxation of the holes as functions of field and temperature. The g factors of the electrons and holes are accurately measured as a function of well width. The role of quantum confinement on the stability of the hole spin is discussed, with particular attention given to the observed ability of the transient hole-exchange field to coherently rotate a macroscopic ensemble of local Mn^{2+} moments. This ''tipping pulse'' initiates a free-induction decay in the sublattice of Mn^{2+} spins and enables electron paramagnetic resonance (EPR) studies of the fractional monolayer magnetic planes. These time-domain EPR measurements reveal a significant magnetic field dependence of the Mn transverse spin relaxation time. [S0163-1829(97)02535-6]

I. INTRODUCTION

Pulsed spin-resonance techniques are powerful experimental tools aimed at the recovery of dynamical information in polarizable materials through the response of a spin system to a ''δ-function'' tipping pulse. The measured spin-relaxation rates, precession periods, and saturation recovery times elucidate a variety of static and dynamic material parameters such as structural information, chemical shifts, and crystal fields, as well as dephasing and dissipation mechanisms. In semiconductor heterostructures, spin resonance techniques are often hindered by the limited signal levels inherent in nanometer-scale quantum-confined systems and by the extremely rapid spin-relaxation times of electrons and holes. Rather, a variety of time-resolved optical techniques, which can energetically pinpoint specific optical transitions in the region of interest, have been developed in recent years to monitor the spin dynamics of photoexcited electrons, holes, and excitons in semiconductor quantum wells.[1–4] Recent interest in nanometer-scale magnetic semiconductor structures, which exploit the spin degrees of freedom in a crystal sublattice of magnetic ions, has benefited greatly from these optical techniques. Femtosecond-resolved studies of exciton spin scattering and dephasing in magnetic heterostructures[5–7] are shedding light on how populations of spin-polarized electronic carriers interact with a matrix of local magnetic moments. In an effort to combine the utility of time-resolved optical methods with the power of traditional spin-resonance techniques, we recently introduced an all-optical method for initiating and measuring free-induction decays of photoinjected electrons and of the local moments (Mn^{2+}) in magnetic semiconductor quantum wells in transverse magnetic fields.[8] The recovery of these oscillatory transients complements existing data taken in longitudinal fields by distinguishing between electron and hole spin relaxation, by identifying the Zeeman splitting of the electrons alone, and by revealing a mechanism by which the electronic carrier spins couple to the magnetic Mn^{2+} moments.

In this paper, we describe a method of time-resolved Faraday rotation to study the dynamic spin behavior of both photoinjected excitons and of the embedded magnetic sublattice. The technique permits measurement of pump-induced changes to the net carrier spin and sample magnetization from femtosecond to microsecond time scales with excellent signal to noise.[5,9] In transverse applied magnetic fields (Voigt geometry, $\vec{H} \perp \hat{c} \| \hat{z}$, where $\vec{H}$ is the applied magnetic field, $\hat{c}$ is the growth axis, normal to the quantum well plane, and $\hat{z}$ is the direction of optical excitation), the selection rules governing optical transitions are modified as compared with the more familiar case of longitudinal fields (Faraday geometry, $\vec{H} \| \hat{c} \| \hat{z}$). Spin eigenstates in the Voigt geometry are quantized in the plane of the quantum well along the transverse field ($\vec{H} \| \hat{x}$), perpendicular to the direction of laser excitation ($\vec{k} \| \hat{z}$). Photoinjected populations of electrons, ini-

tially spin polarized normal to the quantum well plane, are observed to precess about the orthogonal applied field at field-tunable terahertz frequencies, permitting precise measurement of the enhanced electron g factor in these magnetic quantum wells. Comparison with the exciton Zeeman splitting (measured in the Faraday geometry) also allows identification of the hole g factor, completely specifying the relative strengths of the s-d and p-d exchange interaction. The electron and hole g factors are found to decrease in concert as a function of decreasing well width, due to a reduction of the overlap between the carrier wave functions and the regions of magnetic moments.

In contrast to the electrons, the hole spins are not observed to precess. Rather, in narrow quantum wells the hole spins are constrained to lie normal to the quantum well plane (along the direction of observation) by the effects of quantum confinement. With increasing transverse fields the light- and heavy-hole bands become strongly mixed, leading to rapid hole spin relaxation. Due to their distinct temporal evolutions, the electron and hole spin relaxations can be separately identified and the effects of carrier density, temperature, applied field, and magnetic environment on the electron and hole decay are examined. Concurrent time-resolved and spectrally resolved absorption measurements illuminate the processes involved in carrier spin relaxation and reveal a strong dynamic splitting between exciton spin states in zero field. On longer time scales, the magnetic sublattice is coherently perturbed by the torque on the local magnetic moments generated by the transient hole-exchange field. This ''tipping pulse'' rotates the sample magnetization vector away from the axis of the applied field and initiates a free-induction decay in the magnetic sublattice, which persists for hundreds of picoseconds (long after the carriers have recombined). The measured decay of the oscillatory signal is the transverse spin relaxation time of paramagnetic Mn^{2+} spins as measured in traditional electron paramagnetic resonance (EPR) studies, and thus we are able to perform all-optical time-domain spin-resonance studies of fractional magnetic monolayers in quantum-confined geometries. Analysis of the Mn^{2+} oscillation's initial phase and amplitude support the proposed model of coherent rotation and indicate an increased stability of the hole spin in narrower quantum wells. Finally, we investigate the EPR transverse spin-relaxation rates observed in quarter-monolayer MnSe planes, which reveal a marked field dependence.

This paper is organized as follows: Section II details the series of digital magnetic quantum wells, their linear absorption spectra, and the optical selection rules in both longitudinal and transverse magnetic fields. Section III discusses the method of time-resolved Faraday rotation and describes the zero-field and longitudinal-field dynamic responses of photoinjected excitons. In Sec. IV, the ultrafast spin dynamics of electrons and holes in transverse fields are presented. Section V focuses on the induced free-induction decay of the Mn sublattice and presents the results of electron-paramagnetic-resonance experiments. The conclusions are summarized in Sec. VI.

II. SAMPLES AND STATIC MEASUREMENTS

A. Digital magnetic quantum wells

Our samples are wide-band-gap $ZnSe/Zn_{0.80}Cd_{0.20}Se$ molecular-beam-epitaxy- (MBE-) grown single quantum wells, within which are incorporated discrete fractional monolayer planes of the binary magnetic semiconductor MnSe. The quantum well region hence consists of monolayers of the randomly diluted quartenary alloy (Zn,Cd,Mn)Se separated by nonmagnetic layers of $Zn_{0.80}Cd_{0.20}Se$. The ''digital'' distributions of the magnetic Mn^{2+} ions allow great flexibility in designing magnetic heterostructures with specific magnetic environments, while providing direct control over such factors as the shape of the electronic wave function and the local in-plane spin density.[7] Like their diluted-magnetic-semiconductor alloy counterparts, the introduction of magnetic ions into the crystal lattice greatly enhances the effective g factors of the electron and hole bands through the strong spin-sensitive $J_{sp\text{-}d}$ exchange interaction between the s-like (p-like) conduction (valence) band and the local $3d$ electrons that comprise the spin-5/2 paramagnetic Mn^{2+} moment.[10]

In previous experiments, we studied the effects of successive division of a *fixed* number of Mn spins in otherwise identical quantum wells and found that the exciton g factors and spin-scattering rates in longitudinal fields increased significantly as the MnSe planes were further distributed, due largely to the increased overlap of the excitonic wave function with regions of magnetic material, and the larger number of uncompensated Mn^{2+} moments at the heterointerfaces.[7] It was also observed in optical spin-resonance experiments (in transverse fields) that the larger *local* magnetic densities in thicker MnSe planes displayed increased dephasing rates of the Mn^{2+} free-induction decay due to ion-ion exchange interactions.[8]

In the present experiments we maintain a fixed local magnetic environment and vary the quantum well width in an effort to identify the role of quantum confinement on the spin relaxation of electronic carriers in a constant-density matrix of magnetic moments. The samples are fabricated by molecular beam epitaxy on (100) GaAs substrates at a substrate temperature of $\sim$300 °C with 7000 Å buffer and 1000 Å cladding layers of ZnSe. Each of the four samples contains a single quantum well with quarter-monolayer planes of MnSe, spaced by 2.75 monolayers of $Zn_{0.80}Cd_{0.20}Se$. The samples contain 3, 6, 12, and 24 quarter-monolayer magnetic planes, for net widths of $\sim$30, 60, 120, and 240 Å, respectively. Excitons in each structure experience similar magnetic environments, although the binding and exchange energies increase with decreasing well width. In addition, a 120-Å $ZnSe/Zn_{0.80}Cd_{0.20}Se$ nonmagnetic quantum well was grown as a control. The monitoring of oscillations in specularly reflected 12 keV electrons during growth allows the calibration of ZnSe, $Zn_{0.80}Cd_{0.20}Se$ and MnSe growth rates with a reproducibility of $\sim$10% from sample to sample. We note that during the growth of the fractional MnSe layers, there are no other atomic fluxes incident on the sample surface. While the detailed nature of the MnSe nucleation and subsequent surface diffusion cannot be assessed at this stage, the growth mode employed likely favors the formation of MnSe islands. X-ray-diffraction studies of thick epilayers of such digital alloys show distinct superlattice peaks. In conjunction with magneto-optical studies of systematically varied digital quantum wells and transport studies of doped DMH epilayers,[11] these x-ray measurements suggest that the interdiffusion profile of Mn atoms in such digital structures

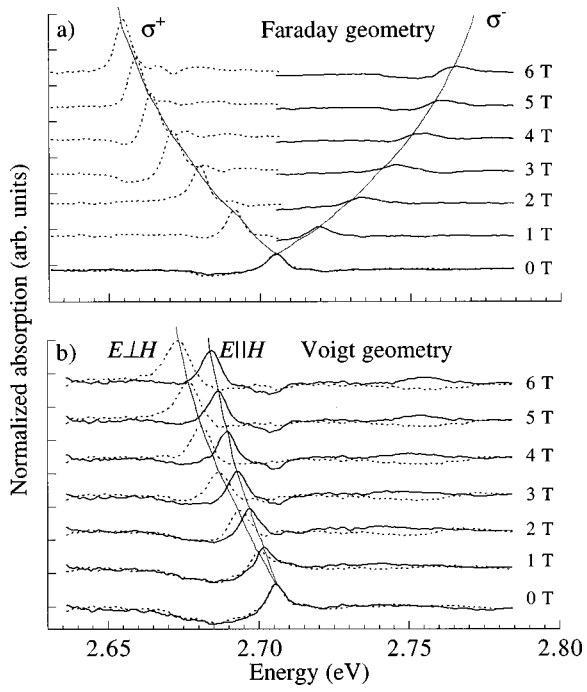

FIG. 1. Normalized absorption spectra of the 240-Å ZnSe/ZnCdSe(MnSe) digital magnetic quantum well at $T=5$ K. (a) In the Faraday geometry ($\vec{H}\|\hat{c}\|\hat{z}$, where $\hat{c}$ is the growth axis and $\hat{z}$ is the observation direction), the σ^+ (σ^-) polarization state is right- (left-) circularly polarized. (b) In the Voigt geometry ($\vec{H}\|\hat{x}$), the two absorption resonances are linearly polarized orthogonal and parallel to the applied magnetic field. Spectra at different fields are offset for clarity.

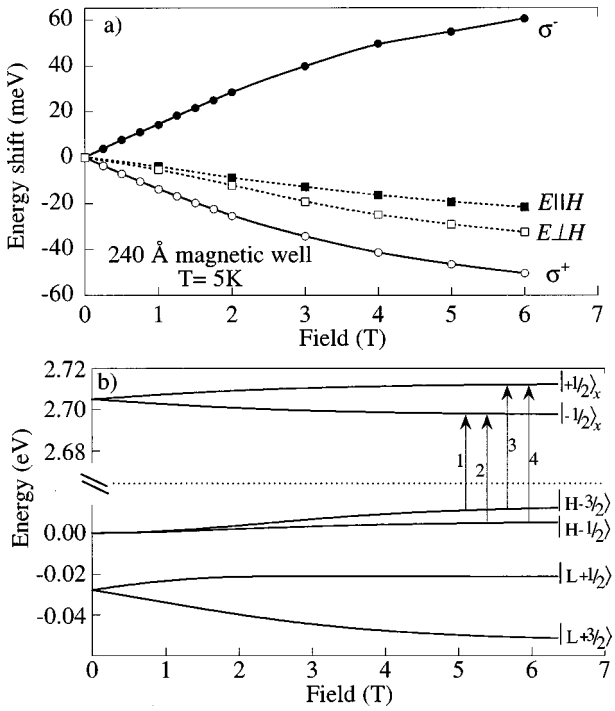

FIG. 2. (a) Measured field-dependent energy shifts of the absorption resonances shown in Fig. 1 for the Faraday (solid lines) and Voigt geometry (dotted lines). (b) Calculated band splittings and optical selection rules in the Voigt geometry ($\vec{H}\|\hat{x}$) for the 120-Å magnetic well, showing the isotropic splitting of the conduction band and the anisotropic Zeeman pattern of the valence band, which arises from competition between the Zeeman energy and the confinement potential. The spins of the heavy- (H) and light- (L) hole mixed valence bands are labeled in a basis along $\hat{x}$, which becomes exact only in the limit of large Zeeman splittings.

has a width of ~1.5 monolayers. Hence, in the present series of samples, we may view each digital MnSe region as a diluted quasi-two-dimensional (quasi-2D) square lattice of antiferromagnetically interacting spins. Static magneto-optical studies of these samples indicate that they remain paramagnetic down to 300 mK.

B. Longitudinal magnetic fields

In the presence of longitudinal applied magnetic fields, low-temperature (5 K) static luminescence and absorption measurements show strong heavy-hole exciton resonances with linewidths of 6–10 meV. No evidence of light-hole or higher-lying resonances is seen. As shown in Figs. 1(a) and 2(a), the fundamental hh exciton is Zeeman split by $\Delta E > 100$ meV at 6 T in the widest magnetic well. The ''effective'' exciton g factor $g_z^{\rm ex}$, defined through $\Delta E = g_z^{\rm ex}\mu_B H_z$, characterizes the magnitude of the splitting in fields parallel to $\hat{z}$ and ranges from $g_z^{\rm ex}=330$ in the narrowest 30-Å well to $g_z^{\rm ex}=490$ in the 240-Å well. The observed increase in Zeeman splitting with well width originates in an increased overlap of the exciton wave function with the magnetic MnSe planes. Note that to lowest order $g_z^{\rm ex}=g_z^e+3g_z^{hh}$, the sum of the individual electron and heavy-hole effective g factors in longitudinal fields. Characteristic magnetoabsorption data taken from the widest quantum well are shown in Fig. 1(a), where the Zeeman splitting of the hh-excitonic resonance is clearly seen. The magnitude of this spin splitting tracks the magnetization of the sample, which follows the expected Brillouin function dependence for spin-5/2 paramagnetic Mn^{2+} ions. The optical selection rules for these and other zinc-blende semiconductors (e.g., GaAs) in longitudinal magnetic fields are well known.[12] In this Faraday geometry, the $\vec{J}=1/2$ conduction band and $\vec{J}=3/2$ heavy-hole valence band are spin split according to g_z^e and g_z^{hh}, and the lower-energy ($S_z=+1$, ''spin-down'') exciton couples to σ^+ circularly polarized photons, while the higher-energy ($S_z=-1$, ''spin-up'') exciton couples to oppositely handed σ^- polarized light.

C. Transverse fields and Voigt selection rules

The experiments presented in the first half of this manuscript center on the measurement of electron spin coherence and hole spin relaxation following injection of spin-polarized carriers with circularly polarized, broadband femtosecond pulses of light in the Voigt geometry. A clear picture of the band-to-band optical selection rules of quantum-confined excitons in the presence of transverse applied fields is required in order to extract meaningful interpretation of the data. Optically allowed transitions in the Voigt geometry are quite different as compared with those in the Faraday geometry, as shown in Fig. 1(b). With increasing field in the quantum well plane, two clearly visible states emerge which both decrease in energy and which are predominantly linearly polarized parallel and orthogonal to the applied field. The energy shifts

of the main absorption peaks for both Faraday and Voigt geometries are plotted in Fig. 2(a). These asymmetric energy splittings in the Voigt geometry are the direct result of 2D spin quantization of heavy holes in quantum wells and the competition between this initial confinement potential and the Zeeman energy.

The reduction from cubic to tetragonal crystal symmetry produced by the in-plane compressive strain and quantum confinement results in the preferred $\hat{z}$ direction for quantization of both spin and orbital angular momenta in the valence bands.[13] Specifically, the heavy-hole spins are projected normal to the quantum well plane and the light-hole spins project in the plane of the quantum well. This spin quantization phenomena originates in the strong spin-orbit interaction of the hole bands, which couples the spin and orbital motion so that (for heavy holes) both are projected along the $\hat{z}$-confinement axis. This effect, as detailed in earlier work with 2D hole gases in strained heterojunctions,[13] results in a vanishing Zeeman splitting of heavy holes in small transverse fields.

Physically, the heavy-hole spins are constrained to lie normal to the quantum well plane (along $\hat{z}$) and the strength of the confinement potential can be quite large in narrow quantum wells, leading to hh-lh splittings in the tens of meV. With the application of a sufficiently large transverse magnetic field, the holes experience a reorientation of their total angular momentum from the growth direction ($\hat{z}$) to the field direction ($\hat{x}$). The relevant field scale is set by the magnitude of the Zeeman energy compared to the confinement potential, and this field scale increases with decreasing well width. In magnetic quantum wells the strong $J_{p\text{-}d}$ coupling leads to very large Zeeman energies which rapidly overcome the large hh-lh splittings in fields of order 1 T. In effect, there is a competition between the hole's initial quantization along $\hat{z}$ due to the confinement potential and the Zeeman energy which would orient the hole spins along $\hat{x}$. No ''good'' quantization axis exists in this intermediate regime; the hole bands are coupled and become mixed, and excitonic transitions radiate into an admixture of circular and linear polarizations. In the limit of very large Zeeman energies (or, alternatively, very wide bulklike quantum wells), the hole spins are entirely oriented along the transverse field, the valence bands can be diagonalized in a basis along $\hat{x}$, and the exciton states couple to linearly polarized light.

The mathematics detailing this anisotropic Zeeman pattern in magnetic quantum wells[14–16] and strained epilayers[17] in transverse magnetic fields has been described in detail. Figure 2(b) shows the results of a calculation of the splitting of the electron and hole bands in the 120-Å magnetic quantum well. The bands are labeled by their representation in a basis along $\hat{x}$, which for the mixed heavy- and light-hole valence bands is exact only in the limit of large Zeeman energies. The two strong resonances observed in Fig. 1(b) correspond to transitions (1) and (2) in Fig. 2(b), and their energy difference is a measure of the energy splitting of the uppermost two hole bands. In the majority of our optical spin-resonance experiments, circularly polarized optical pulses are used to inject excitons from the upper two hole bands with definite spin along the $\hat{z}$ axis. This necessarily corresponds to exciting a superposition of transitions (1)–(4). Electrons with definite $S_z^e=|\frac{1}{2}\rangle_z$ correspond to a coherent superposition of the states $S_x^e=|\pm\frac{1}{2}\rangle_x$, and holes with $J_z^{hh}=|\frac{3}{2}\rangle_z$ are created from a superposition of the mixed bands $|H-\frac{3}{2}\rangle$ and $|H-\frac{1}{2}\rangle$. The coherence of the superposition of mixed hole states decays rapidly and corresponds to a rapid spin relaxation of the holes. The distinct electron bands preserve their *intraband* coherence over much longer time scales, and a temporal evolution of this coherent superposition corresponds to a classical precession of the electron spin about the applied field.

III. CARRIER SPIN DYNAMICS IN ZERO FIELDS AND LONGITUDINAL FIELDS

A. Experimental design

Faraday rotation is the phenomenon by which the linear polarization of a laser directed along $\vec{k}$ through a magnetized medium will be rotated by an amount proportional to the component of magnetization along $\vec{k}$. The rotation originates in the fact that a sample magnetization along $\vec{k}$ presents different indices of refraction for left- and right-circularly polarized light. In addition, the presence of unequal populations of photoexcited carriers in the two spin states (σ^-,σ^+) affects the indices of refraction unequally and also leads to a measured Faraday rotation. In this way the measurement is sensitive to the net spin of the photoexcited carriers. Extending these results to the time domain, we measure the pump-induced changes to the Faraday rotation of a time-delayed probe. As such, the method allows a femtosecond-resolved measurement of net carrier spin and also of any induced perturbations to the underlying magnetic moments in a sample, which may persist long after all carriers have recombined.

In preparation for time-resolved Faraday rotation measurements, the samples are epoxied facedown on fused silica slides and the opaque GaAs substrates are mechanically thinned, polished, and chemically removed with a powerful spray etch down to the ZnSe buffer layer. The etched structures are mounted in an split-coil (0–8 T) magneto-optical cryostat with a variable-temperature insert (1.5–300 K). The output from a Ti:sapphire laser is frequency doubled in an external BBO crystal, giving 120-fs optical pulses in the 440–510 nm range. The laser energy is tuned to the hh-exciton resonance energy. The 76-MHz repetition rate of the optical pulse train is reduced with a synchronous external acousto-optic pulse picker. The pulse picker is adjusted to diffract every 40th optical pulse, reducing the repetition rate of the optical pulse train to $\sim$2 MHz. This reduction is essential in the study of magnetic systems, where the magnetic recovery times can be of order 1 μs. The pulse train is split into pump and probe beams, which are separately polarized, time delayed, mechanically chopped and/or modulated, and directed to the cryostat. Typical average powers are 100 μW in the pump beam and 3 μW in the probe. We estimate roughly 5×10^6 excitons created per pump pulse or $\sim10^{11}$ excitons/cm^2.

As shown in Fig. 3(a), the circularly polarized pump pulse excites an initially spin-polarized population of electrons and holes, and the ''instantaneous'' net carrier spin or sample magnetization *along* $\hat{z}$ is measured as a function of time delay through the Faraday rotation imparted to the weak,

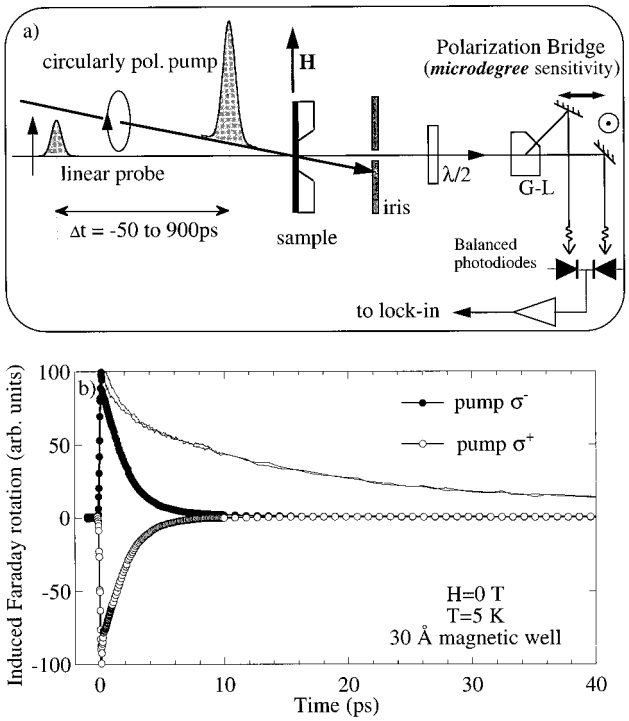

FIG. 3. (a) Experimental schematic, showing the balanced photodiode bridge. (b) Zero-field time-resolved Faraday rotation showing rapid spin relaxation of excitons in response to photoexciting the σ^+ or σ^- state, as measured by the difference in photodiode currents. Also shown (thin lines) is the much longer, polarization-independent carrier recombination time, as measured by the sum of the photodiode currents.

linearly polarized probe. Extremely sensitive measurements of the induced Faraday rotation (10^{-6} rad) are made using a balanced diode bridge.[9] With the pump blocked, the broadband half-wave plate rotates the transmitted probe beam to 45° with respect to the Glan-Laser polarization beam splitter, giving equal insensities in both arms of the bridge and a null signal in the difference of the two photodiode currents. To first order all laser noise is canceled out with this detection scheme. The small pump-induced deviations from this null condition constitute the signal and are measured with lock-in amplifiers.

In Fig. 3(a) the applied magnetic field $\vec{H}$ is drawn along $\hat{x}$ or in the plane of the quantum well. Switching from this Voigt configuration to the case of longitudinal fields (Faraday geometry, $\vec{H}\|\hat{z}$) involves only a 90° rotation of the field. In some of the experiments to be discussed, mechanical chopper wheels are used in the pump beam to enable lock-in detection, and in this way we measure the Faraday rotation induced by the photoinjection of a particular orientation of exciton. We alternately use a high-frequency photoelastic modulator to modulate the pump between right- and left-circular polarizations, and in this way only the part of the signal that depends explicitly on the photoinjected spin orientation (pump orientation) is recorded.

B. Time-resolved Faraday rotation in zero field

In zero applied magnetic field, photoexcitation with either right- or left-circularly polarized light results in an initially spin-polarized exciton population. As shown in Fig. 3(b), the pump-induced Faraday rotation signal measures the net carrier *spin*, which decays rapidly to zero after a few picoseconds as the excitons and their constituent electrons and holes spin-flip scatter and equilibrate between the nominally degenerate spin states. Pumping with the opposite handedness of circularly polarized light shows the expected sign reversal of the Faraday rotation signal. The excitons themselves recombine on much longer time scales, as is verified by simultaneously measuring the sum of the photodiode currents. This measurement records the exciton lifetime through the pump-induced changes in the total transmission of the linear probe and is sensitive to the net *number* of carriers (which bleach the transitions due to phase-space filling effects). As shown by the thin lines in Fig. 3(b), this transient absorption is long lived and independent of the handedness of the optical pump, as expected.

In general, the measured decay of the Faraday rotation is not purely exponential. Much experimental[2] and theoretical[18] work has been aimed at understanding the spin relaxation of resonantly pumped excitons in quantum wells. Separate contributions have been identified for individual hole and electron spin flips, which take optically active $J_z=\pm 1$ excitons to ''dark'' $J_z=\pm 2$ states, as well as exciton spin flips between optically active states in which the electron and hole spin flip together in an interaction mediated by the exchange energy between them. Other scenarios, such as enhanced radiative recombination of excitons on short time scales[19] and spectral diffusion of excitons away from $|\vec{k}|=0$, have been considered.[20] A quantitative analysis of our observed Faraday rotation decay, which in these magnetic systems must certainly also include the role of the local Mn^{2+} moments, is beyond the present scope of this paper. Rather, our aim is to illustrate the general trends of spin relaxation present in magnetic quantum wells in the presence of applied fields and, more importantly, to demonstrate that in transverse magnetic fields precessing moments permit clear identification of electron spin dynamics distinct from the dynamics of the holes.

In the present series of digital magnetic quantum wells, the spin-relaxation signals measured in transient Faraday rotation contain no contribution from interband (conduction-valence) coherence effects, which are found to occur on time scales faster than the experimental resolution of ~250 fs. In general, resonant excitation of semiconductors with ultrafast pulses induces a coherent polarization between the valence and conduction bands, which decays rapidly as the excitons lose memory of the optical excitation phase through momentum-, spin-, and energy-relaxation processes. This *interband* coherence is explicitly measured in coherent optical spectroscopies such as four-wave mixing or in pump-probe experiments where the incident laser polarizations specify sensitivity to coherent polarization decay. Interference between polarization decays, arising from coherent excitation of more than one optical transition, results in quantum beats.[3,21] Measured time scales for interband coherence in III-V and nonmagnetic II-VI quantum wells are typically <5 ps, but vary dramatically with sample quality and the specifics of sample growth which, for example, may (inadvertently) lead to roughening of the heterointerfaces and localization of the excitons. It has been observed that localized excitons in disordered samples maintain their phase much

longer than in higher-quality samples where the wave function is spatially extended,[22,23] due to a reduction in phase-breaking exciton-exciton scattering events. Furthermore, the inclusion of magnetic moments into II-VI quantum wells is found to greatly accelerate exciton phase relaxation, although with suprisingly little dependence on applied field.[6] Coherent polarization ''spin beats'' have been measured in magnetic II-VI quantum wells with transient Faraday rotation experiments,[24] yielding fast dephasing times of <1 ps. These samples exhibited broad ($\sim$15 meV) inhomogeneous linewidths, long spin lifetimes ($>$70 ps), and weak coupling with the magnetic sublattice (evidenced by small effective g factors $g^{\mathrm{ex}} \approx 30$), suggesting an exciton population that was largely localized. Nominally identical samples grown later with improved MBE techniques showed narrow ($\sim$6 meV) linewidths, strong coupling with the magnetic ions ($g^{\mathrm{ex}} \approx 190$), and fast spin relaxation ($\sim$5 ps) and exhibited no sign of interband coherence outside of the 250-fs experimental time resolution.[25] Our present series of magnetic wells are of this latter variety, and the static and time-resolved data indicate high-quality samples and delocalized excitons with extended wave functions encompassing a large number of local Mn moments, as evidenced by the greatly amplified g factors, increased rate of spin scattering, and ''instantaneous'' ($<$250 fs) dephasing of the induced interband coherence.

C. Time-resolved and spectrally resolved absorption in zero field

Further insight into the exciton spin dynamics in zero field is gleaned from the time-resolved and spectrally resolved absorption of the two spin eigenstates. Following resonant excitation of the $J_z = +1$ exciton with a σ^+ circular pump pulse, the induced absorption of σ^+ and σ^- probe light is measured as a function of wavelength and time delay. The bandwidth of the laser ($\sim$4 nm at 470 nm) is sufficient to encompass the entire exciton resonance, and the transmitted probe beam is dispersed in a scanning monochromator and detected with a photomultiplier tube. Figure 4(a) shows the pump-induced absorption immediately following σ^+ excitation, well before appreciable spin scattering can populate the σ^- state. Regardless, the data clearly show that both spin states are immediately affected: The σ^+ resonance has blueshifted to higher energy, and the σ^- state has redshifted to lower energy (negative signal or induced absorption on the low-energy side indicates a redshift and vice versa). The larger positive signal in the case of a copolarized pump and probe (solid line) reflects the additional induced transmission due to bleaching of the σ^+ exciton resonance through phase-space filling (PSF) effects. Thus the differences between the two traces are indicative of imbalanced exciton spin populations. As the excitons scatter and the net carrier spin approaches zero, the two traces collapse on top of one another and are identical by 50 ps, as shown in Fig. 4(b). With equal population in each spin state, the energies are again degenerate and the observed signals simply reflect carrier populations through bleaching and a slight broadening of the exciton resonance. With the detection wavelength at the spectral peak of the induced transmission, the two spin states evolve in time as shown in Fig. 4(c). Spin-dependent effects account

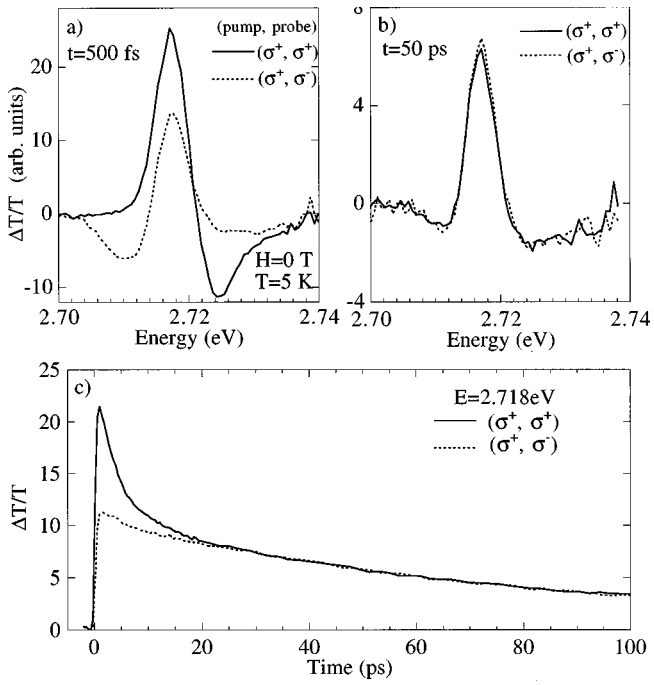

FIG. 4. Zero-field time-resolved and spectrally resolved absorption of the individual exciton spin states. Spectra are taken (a) immediately following excitation and (b) at 50 ps, after spins have equilibrated. (c) A time scan at the peak of the exciton resonance showing fast spin equilibration followed by slower exciton recombination.

for the difference between the two curves, and following complete spin relaxation by $\sim$20 ps, the identical decays are simply given by the carrier recombination time. The dynamic blueshift and redshift observed at short time delays have been measured and discussed in detail in GaAs quantum wells and are elegantly explained[26,27] as the mutual repulsion (attraction) of excitons with similar (opposite) spin. Excitons are composed of fermions, and the interaction between the constituent electrons, much like molecular hydrogen, is repulsive (antibonding) for similar spins and attractive (bonding) for opposite spin.

D. Time-resolved Faraday rotation in longitudinal fields

The spectral information revealed by the transient absorption technique complements the Faraday rotation data, but lacks the signal to noise afforded by the balanced diode bridge. Superior noise rejection is essential in measuring the extremely small pump-induced perturbations to the magnetic sublattice that arise when transverse magnetic fields are applied. Some of the features seen in transverse fields are more readily explained, however, with a clear understanding of the longitudinal-field case shown in Fig. 5. In longitudinal magnetic fields, the energy degeneracy between the $J_z = \pm 1$ excitons is lifted and the lower-energy spin-down exciton state becomes energetically favorable. The induced Faraday rotation signal, shown for the narrowest magnetic well, develops a pronounced asymmetry resulting from the preferential spin scattering of excitons into this lower-energy state. Spin scattering from the σ^- state to the σ^+ state is enhanced, and after $\sim$2 ps the majority of the injected σ^- excitons have flipped to the σ^+ eigenstate, as evidenced by the negative

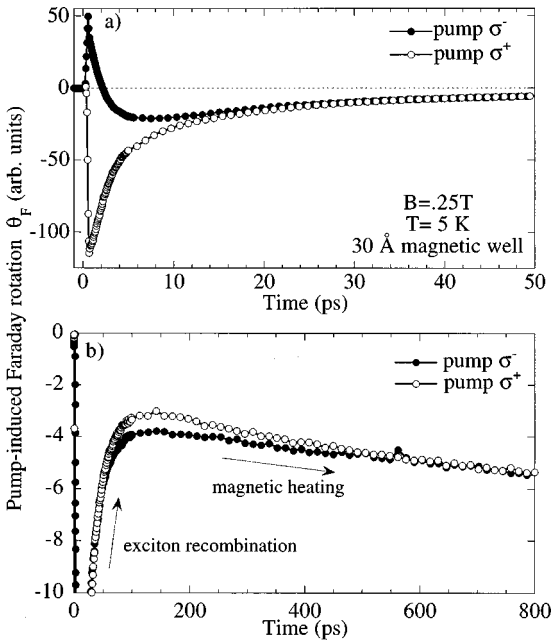

FIG. 5. Time-resolved Faraday rotation in small longitudinal magnetic fields (Faraday geometry), showing (a) on short time scales the excitons preferentially scatter to the σ^+ state, and thermalize by 20 ps. (b) At longer times, the excitons recombine and the magnetic sublattice dynamically warms slightly over hundreds of picoseconds.

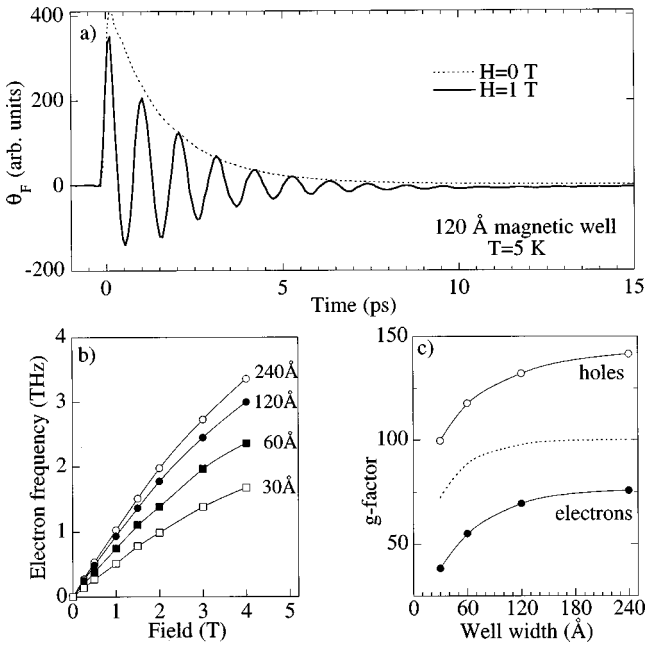

FIG. 6. (a) Time-resolved Faraday rotation in transverse magnetic fields (Voigt geometry), showing strong electron spin beats which follow the zero-field envelope. (b) The electron Larmor precession frequency vs field in the different well-width samples. (c) Measured electron and hole g factors as a function of well width. The dotted line is a calculation of the carrier wave function overlap with the planes of MnSe (arbitrarily scaled).

sign of the Faraday signal. Conversely, spin scattering out of the favorable σ^+ state is suppressed. The initial spin-scattering rates in these samples appear to be driven thermodynamically by the Zeeman splitting between the exciton states, similar to previous measurements.[7] Regardless of pump orientation, the relative exciton populations achieve complete equilibrium after ~20 ps in this sample. This equilibrium state, corresponding to a majority of excitons in the lower-energy state and a negative induced Faraday signal, corresponds to a net *decrease* or *reduction* in the total sample magnetization. The σ^+ exciton spins are oriented antiparallel to the longitudinal field, resulting in a small transient demagnetizing field in the sample.

As the excitons recombine, the net carrier spin measured through the Faraday signal decays to zero. However, this decay terminates after ~100 ps and the signal begins to slowly increase in the negative direction [Fig. 5(b)]. This nonzero, pump-orientation-*independent* long-lived signal is direct evidence of the dynamic heating of the Mn^{2+} spin sublattice, which reduces the net sample magnetization in accordance with the Brillouin function. The observed signal shape in Fig. 5(b) is simply the superposition of the decay of the few remaining excitons and the slow rise from zero of the warming Mn moments (the slight difference between the two traces is an experimental artifact—data taken with the polarization modulator verify that this difference is identically zero beyond ~20 ps. The dynamic heating of the Mn^{2+} moments, which occurs on ~300 ps time scales, saturates at a value which scales roughly with temperature as T^{-2} in a constant applied magnetic field and as T^{-1} in constant Zeeman splitting (sample magnetization). The final cooling of the Mn sublattice back to equilibrium temperature proceeds through spin-lattice relaxation and requires hundreds of nanoseconds or even microseconds depending on the temperature.[9]

In no case have we observed a long-lived, *spin-dependent* magnetic response in the present series of digital magnetic quantum wells in longitudinal fields. There is no evidence that the spin-polarized carriers directly impart any persistent or long-lasting angular momentum to the magnetic sublattice through the carrier-ion spin interaction ($J_{sp\text{-}d}\vec{S}\cdot\vec{s}$). Instances of optically induced magnetization in magnetic semiconductors are not uncommon, however: The diagonal or mean-field part of this interaction ($S_z s_z$) has been identified in polaron formation[28] and in photoinduced magnetization studies.[29] Similarly, the off-diagonal or ''spin-flip'' terms ($S_+ s_- + S_- s_+$) are thought to be responsible for the long-lived magnetizations observed in earlier time-resolved Faraday rotation experiments on weakly coupled magnetic samples.[24] It will be important to distinguish these mechanisms from those which induce the long-lived *oscillatory* magnetizations which occur in transverse applied fields, as discussed in Sec. V.

IV. TRANSVERSE APPLIED FIELDS

A. Electron Larmor precession

When the applied field is rotated to lie in the plane of the quantum well ($\vec{H}\|\hat{x}$), strong oscillations appear in the measured Faraday rotation [Fig. 6(a)] that result from electron precession about the field axis. In this situation, electrons and holes are photoinjected into the quantum well with their spins initially oriented normal to the quantum well plane

($\vec{S}^{e,h}\|\hat{z}$). The electron spins precess about the applied field with a Larmor frequency determined by the electron spin splitting in transverse fields. Quantum mechanically, injection of electrons with definite initial S_z corresponds to the creation of a coherent superposition of the spin-split electron eigenstates which are quantized along $\hat{x}$, $|S_x=+\frac{1}{2}\rangle \pm |S_x=-\frac{1}{2}\rangle$. The projection of this superposition onto the measured $\hat{z}$ axis will oscillate with time. This population of precessing electrons will also manifest in time-resolved absorption or luminescence measurements, where it was first studied in GaAs,[30] and has since been used to measure electron g factors in various semiconductor compounds.[31] The conduction band in zinc-blende semiconductors is s-like, and so the electron g factor and Zeeman splitting are isotropic ($g_x^e=g_y^e=g_z^e$). Consequently, the frequency of oscillation, $\Omega=g^e\mu_B H_x/\hbar$ enables very precise measurement of the electron g factor alone, which in magnetic quantum wells is amplified manyfold through the strong s-d exchange interaction. The electron Larmor frequency at 5 K for all four magnetic wells is shown in Fig. 6(b). The beat frequency follows the expected Brillouin function, and the corresponding energy splitting at 5 K and low fields indicates $g^e=38.3$, 55.2, 69.6, and 75.8, in order of increasing well width. The increase in g^e with well size, plotted in Fig. 6(c), results from a greater overlap of the electronic wave function with the MnSe planes, which is qualitatively reproduced in a simple 1D Schrödinger equation solution for the particular well geometries (dotted line). Comparison with the Zeeman splittings of the *exciton* spin states measured in the Faraday geometry [see Figs. 1(a) and 2(a)] enables accurate identification of the heavy-hole g factors through $g_z^{\rm ex}=g^e+3g_z^{hh}$. Hole g factors are not isotropic; the valence band is p-like and therefore subject to spin-orbit effects as discussed in Sec. II. Both hole and electron g factors are found to depend strongly and similarly on the quantum well width [Fig. 6(c)].

In direct analogy with the free-induction decays of nuclear spins in NMR, the exponential envelope of the electron spin precession signal indicates the electron transverse spin-relaxation time or, alternatively, the electron *intraband* coherence time. Inhomogeneous dephasing in the magnetic wells, arising from excitons in different regions of the sample experiencing larger or smaller magnetic fields, appear to be insignificant—the envelope closely follows the zero-field spin decay [Fig. 6(a)]. This is an indication that in these magnetic wells the magnetic environment is laterally uniform on length scales larger than the spatial extent of the exciton wave function. Monitoring the envelope decay of the electron beats is a powerful method of measuring the spin relaxation of the electron population alone. As an example of the utility of this method, Fig. 7 shows the effect of excitation density on the spin relaxation and Larmor frequency of the photoinjected electron population. The electron spin-relaxation time increases with higher exciton density and is accompanied by a reduction of the Larmor frequency. The photoinjected carrier density is fairly large—of order 5×10^{11} excitons/cm^2 at the highest pump power, and so the observed effects may be due to screening between the delocalized excitons and their constituent electrons. Slower electron spin-relaxation times at high pump powers have been observed[27] in III-V systems and were attributed to a many-body screening of the electron-hole exchange interaction within an exciton. It is possible that the longer precession period at high carrier densities may be the result of a slight average warming of the magnetic sublattice at higher pump powers, even though the sample was excited only once every microsecond. However, similar results were obtained at higher temperatures (20 K), where magnetic heating effects are reduced. Alternatively, this effect could result from decreased g factors for electrons with large k vectors, as was observed in nonmagnetic GaAs quantum wells.[31] However, a population of electrons experiencing a spectrum of g factors would be expected to dephase more rapidly, in contrast to the observed results.

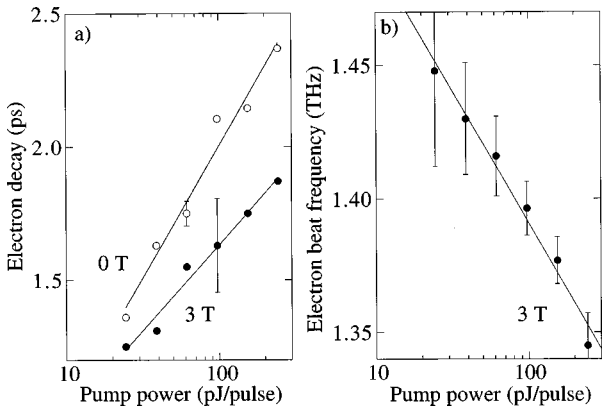

FIG. 7. Pump-power dependence of (a) the electron spin-relaxation time and (b) electron precession frequency in the 30-Å magnetic quantum well at $T=5$ K. Solid lines are guides to the eye.

B. Hole spin-relaxation time

In addition to the precessing electrons, there are an equal number of optically excited holes present in the quantum well, which raises the interesting question of whether or not the data reflect their presence. Previous studies in zero field and in longitudinal fields have revealed monotonic decays of carrier spin that are not single exponential, and separate contributions from electrons, holes, and/or excitons are inferred from the shape and time scale of the decay components.[2,5,18] Alternatively, spin relaxation in n- or p-doped quantum wells identifies the separate contributions from holes and electrons.[27] In the present study using transverse fields, the electron population generates a unique oscillatory signal, so that spin contributions from other sources (holes, magnetic sublattice) can be readily distinguished. The data reveal that after the first few picoseconds following excitation, the signal oscillates about zero, indicating that on these time scales the measured spin dynamics contain *no contribution* from hole or exciton relaxation. Also, because the decay envelope of the beats in the magnetic wells generally follows the zero-field spin relaxation [see Fig. 6(a)], it can be reasonably assumed that electrons account for the ''longer-lived'' spin times in the zero-field double-exponential spin decays observed in these samples, while hole or exciton spin relaxation occurs on the faster time scales.

However, the data immediately following zero time delay show electron oscillations whose average value is offset by a positive, exponentially decaying quantity.[8] This additional contribution to the measured spin dynamics has been inter-

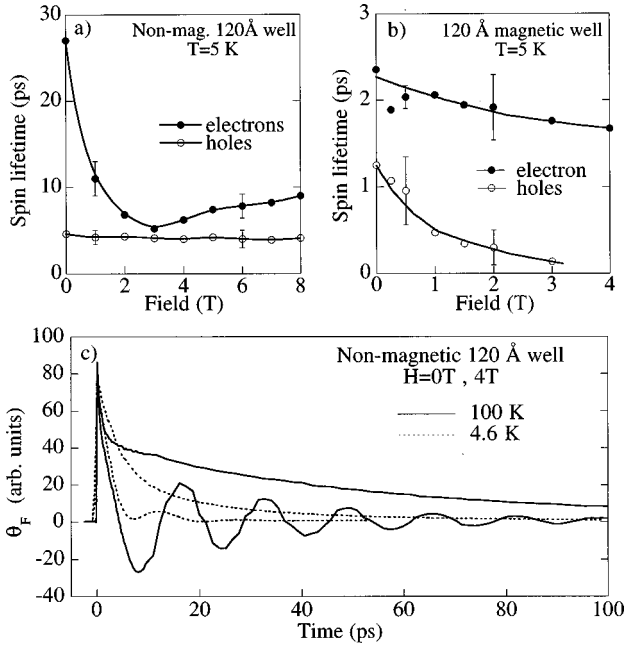

FIG. 8. Measured electron and hole spin-relaxation times in (a) a nonmagnetic quantum well and (b) in a strongly coupled magnetic quantum well. (c) Time-resolved Faraday rotation in the nonmagnetic sample at 4.6 and 100 K, showing much longer electron spin-relaxation times at elevated temperatures.

preted as arising from the very fast spin relaxation of the holes. In the present series of magnetic wells, the measured hole spin-relaxation rates are very rapid in zero field (~1.3 ps) and become faster as the transverse field is applied, until they fall well below the experimental time resolution at ~3 T. Against expectation, the measured hole relaxation times show little difference between the four well width samples, in contrast with our earlier experiments on samples containing varied magnetic environments which showed longer hole spin relaxation with less dependence on field in weakly magnetic and nonmagnetic samples. Evidently, quantum confinement effects play a minor role in determining the hole spin-relaxation dynamics, even though heavy holes in narrow wells are assumed to possess additional stability against scattering by the increased *hh-lh* energy splitting. Rather, the specifics of the magnetic environment (strongly coupled and roughly identical in the present series of samples) seem to determine the fate of the holes, suggesting strong mixing of the valence bands, which is driven by the large magnetically enhanced Zeeman splittings.

C. Temperature and field dependence of transverse spin relaxation

The role of the magnetic sublattice upon the electron and hole spin-relaxation times (τ_e, τ_h) is illustrated in Figs. 8(a) and 8(b), which show representative plots of τ_e and τ_h vs applied field in weakly and strongly magnetically coupled quantum wells at low temperatures. Figure 8(a) shows data from the nonmagnetic $ZnSe/Zn_{0.80}Cd_{0.20}Se$ 120-Å quantum well, where we measure electron and hole spin-relaxation times of 27 and 5 ps in zero field. As the transverse field is increased, τ_h remains largely unchanged, while τ_e shows a dramatic decrease to ~6 ps at 3 T, followed by a slow rise to ~9 ps at 8 T. In contrast, the magnetic sample, which is a 120-Å well containing 12 quarter-monolayers of MnSe, shows nearly the opposite behavior [Fig. 8(b)]: In zero field the spin-relaxation times are much faster: about 2.2 and 1.2 ps for τ_e and τ_h, respectively. With increasing field, τ_e is only weakly affected, whereas τ_h decreases sharply until it becomes too rapid to measure. Figure 8(b) is characteristic of all the strongly coupled magnetic wells we have measured, regardless of well width.

We infer that in zero field the incorporation of local magnetic moments into an otherwise nonmagnetic II-VI quantum well opens new channels for spin scattering which greatly accelerate the measured spin relaxation of electrons and holes. Two mechanisms are considered: alloy disorder spin-flip scattering and magnetic spin-flip scattering. In the former scenario, carrier spins are scattered by the fluctuations in the energy landscape due to the presence of alloy materials [in this case, the monolayers of (Zn,Cd,Mn)Se]. In the latter case, carrier spins interact directly with the local magnetic impurities and flip their spins in an angular-momentum-conserving process. We consider it unlikely that the introduced alloy disorder is responsible for the observed increase in spin-scattering rates. As discussed earlier in this paper, there is evidence that alloy disorder acts to further localize excitons and thus *decrease* spin scattering. Furthermore, in a related four-wave mixing experiment it has been observed that the introduction of nonmagnetic impurities into a II-VI quantum well results in longer exciton phase scattering times, while the introduction of a similar number of *magnetic* impurities leads to very fast dephasing.[6] Thus we believe that the strong coupling (or overlap) between the carriers and the magnetic sublattice which is responsible for the greatly enhanced g factors also directly leads to the rapid spin relaxation of electrons and holes through the dominant channel of carrier-Mn spin-flip processes.

When transverse fields are applied, there appear contrasting trends between spin relaxation in the magnetic and nonmagnetic samples. It is important to recall that the Zeeman splittings in the magnetic sample are two orders of magnitude larger than in the nonmagnetic sample and that this Zeeman energy may dominate certain processes in the magnetic well while remaining insignificant in the nonmagnetic well. As discussed in Sec. II, quantum-confined heavy holes, which are generally thought to undergo spin relaxation by mixing with the light-hole band away fom $k=0$, would not be expected to spin relax faster until the Zeeman energy was commensurate with the *hh-lh* splitting. In the nonmagnetic well the Zeeman energy is always much less than the *hh-lh* splitting, and indeed no dramatic change in the hole spin-relaxation time is observed. On the contrary, the huge Zeeman splitting of the hole bands in magnetic wells readily mixes the hole states in modest magnetic fields [see Fig. 2(b)], leading to the observed strong enhancement of the hole spin relaxation with applied field. However, this scenario would imply that samples with larger well widths, which possess smaller *hh-lh* splittings, would show a faster decrease of τ_h with field, and in fact this is not directly observed within the limits of experimental uncertainty.

To explain the unusual behavior of τ_e vs field in the nonmagnetic sample [Fig. 8(a)], we tentatively suggest the possibility that the observed minimum at 3 T results from the

destabilization of the electron spin, which in low fields is pinned to lie along the growth axis by the exciton exchange energy. This exchange energy ($\sim$250 μeV), which favors antiparallel electron and hole spin alignment, acts as an internal magnetic field along $\hat{z}$ and is equaled by the electron Zeeman energy in this sample at $\sim$3 T. At this point the applied field along $\hat{x}$ can rotate the electron spin away from the growth axis and into the plane of the quantum well, where it may experience increased scattering. By contrast, in the magnetic sample [Fig. 8(b)], the electron-Mn spin-flip scattering dominates over other processes and is relatively insensitive to the applied field.

Temperatures of up to 130 K are found to have little effect on the measured spin-relaxation times in strongly coupled magnetic samples. Although the electron precession frequencies slow considerably at elevated temperatures (in accordance with the Brillouin function), the decay envelope remains almost exactly identical (not shown). In stark contrast, temperatures above $\sim$70 K result in a dramatic lengthening of the electron spin-relaxation time in nonmagnetic wells, as shown in Fig. 8(c) at high temperature. Electron beats now persist for hundreds of picoseconds and roughly follow the zero-field envelope (solid lines), showing no evidence of the rapid decrease in spin-relaxation time seen at 5 K. The hole relaxation time, on the other hand, remains largely unchanged.

In the present series of magnetic quantum wells, the final decay of the electron precession occurs by $\sim$10–25 ps. Beyond this point, the electrons (and holes) have completely relaxed and are oriented along the applied field, giving no Faraday rotation signal in the orthogonal observation direction. The eventual recombination of the excitons ($\sim$100 ps) is invisible to the Faraday rotation method as they project no net spin along the growth axis. However, their presence in the well can be indirectly inferred, as will be discussed shortly.

V. COHERENT ROTATION OF THE Mn SUBLATTICE

A. Free-induction decay of the Mn^{2+} sublattice

Following the complete spin relaxation of the electrons, the data in transverse fields reveal a much smaller oscillatory signal with a completely different period [Fig. 9(a)]. This new signal persists for hundreds of picoseconds [Fig. 9(b)] and results from the free-induction decay of a coherently perturbed ensemble of Mn^{2+} spins precessing about the applied field in synchrony. Note that all photoexcited carriers have recombined completely by 100 ps, and so the long-lived oscillation is purely magnetic in origin. In the absence of a pump pulse, the Mn^{2+} spins are preferentially aligned along the $\hat{x}$ axis of the applied field, where their net magnetization M_x is ''invisible'' to the Faraday rotation probe which measures only induced magnetizations along $\hat{z}$. For this reason, time-resolved Faraday rotation in the Voigt geometry is also insensitive to pump-induced warming of the Mn sublattice (as was seen in longitudinal applied fields) or other changes in the magnitude of M_x. Rather, the observed signal must arise from a macroscopic number of Mn spins having acquired a net magnetization in a direction orthogonal to the applied field. These ''tipped'' Mn spins precess about the applied field, projecting a small field along $\hat{z}$,

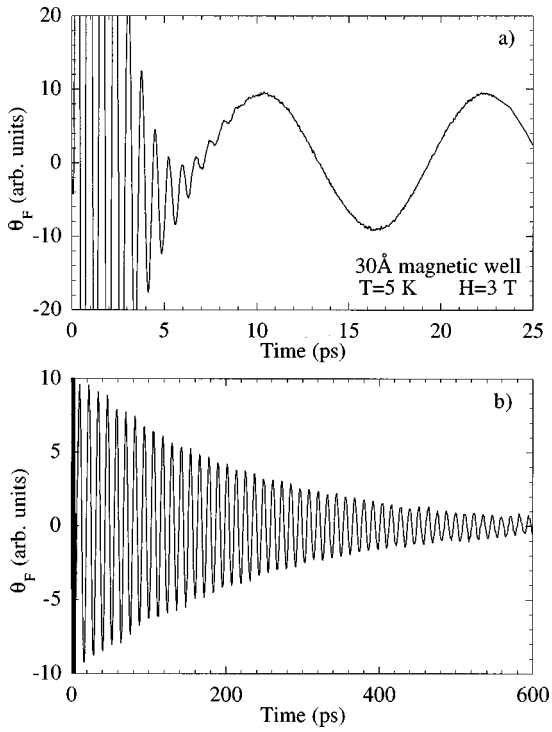

FIG. 9. Time-resolved Faraday rotation in the Voigt geometry, with (a) the last few electron beats, revealing the presence of manganese beats. (b) Expanded view of the Mn^{2+} free-induction decay.

which is measured as a small Faraday rotation. This field oscillates in time as the moments precess and decays away as the ensemble spin scatters or dephases, in direct analogy with nuclear free-induction decays in NMR. The measured oscillation frequency increases linearly with field and corresponds to the accepted Mn g factor equal to 2.01. The signal is absent in the nonmagnetic sample and present (with the same g factor) in every magnetic sample. As expected, the Mn oscillation frequency is independent of temperature, as shown in Fig. 10. Here raising the temperature is shown to reduce the electron Larmor frequency (which follows the Brillouin-like sample magnetization), but have no effect on the frequency of the Mn precession, in agreement with the temperature-independent manganese g factor.

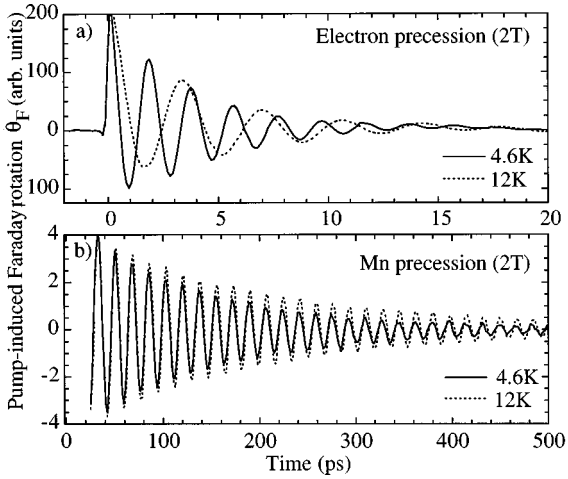

FIG. 10. Free-induction decays of (a) the photoexcited electrons and (b) the Mn^{2+} ions at 4.6 and 12 K.

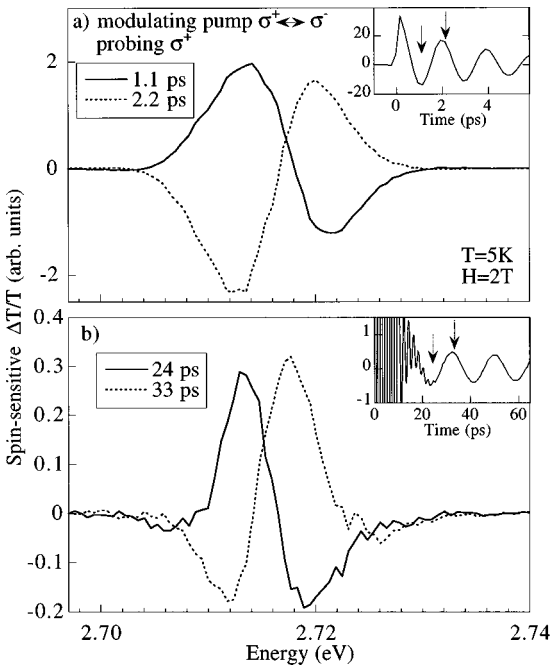

FIG. 11. Time-resolved and spectrally resolved absorption of the individual (σ^+,σ^-) exciton spin states in a transverse applied field. Here the signal is spin sensitive: One measures only the *difference* in induced absorption between pumping with σ^+ and σ^- light. The signals, measured at the times indicated by the arrows in the insets, derive from (a) precessing electron spins which bleach the preferentially occupied spin state and (b) the precessing Mn^{2+} spins which induce an oscillatory Zeeman splitting between the spin states.

Transient absorption measurements help to clarify the origin of the observed Faraday rotation signals by spectrally resolving the absorption resonance shifts of specific polarization orientations. Figure 11 illustrates such a measurement. In this case, the probe is σ^+ polarized and the pump is modulated between σ^+ and σ^- circular polarizations. In this way we record only the *difference* in transient absorption between pumping with σ^+ light and pumping with σ^- light. In effect, this is equivalent to taking the difference between the solid and dotted traces in Fig. 4, and is therefore sensitive only to the net carrier *spin*, rather than the total carrier populations in each spin state. In transverse magnetic fields, the data in Fig. 11(a) show transient absorption spectra taken at the minima (1.1 ps) and maxima (2.2 ps) of the electron oscillations shown in the inset. The data effectively indicate that electrons have precessed halfway around the applied field and now preferentially occupy the opposite spin state, so that the σ^+ and σ^- absorption resonances, which were originally redshifted and blueshifted at 1.1 ps, are now blueshifted and redshifted, respectively, giving the inverted signal at 2.2 ps (the blueshifted state is also preferentially bleached due to phase-space filling). After the electrons have spin relaxed, it is still possible to measure a similar effect in the transient absorption arising from the precession of the Mn moments [Fig. 11(b)]. As the Mn^{2+} ensemble precesses, it projects a small magnetic field onto the measured $\hat{z}$ axis, causing a small oscillatory induced Zeeman splitting between the σ^+ and σ^- absorption peaks. This difference between the two absorption resonances is measured at 24 and 33 ps, where the Mn^{2+} spin ensemble is slightly tilted parallel and antiparallel to the observation direction (along $\hat{z}$). These oscillatory absorption resonances for circulaly polarized light are necessarily associated with their respective dispersion curves $[\eta_+(\lambda),\eta_-(\lambda)]$, and it is the difference between these dispersion curves which is directly proportional to the measured Faraday rotation. As a final note we point out that a comparison between Figs. 11(a) and 11(b) indicates the decreased carrier population—the absorption resonances have narrowed and redshifted at the longer times, where they are no longer broadened by the presence of as many carriers, and PSF effects are reduced.

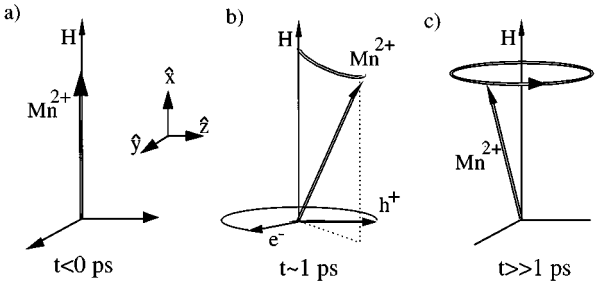

FIG. 12. Model for coherent rotation of the Mn sublattice about the transient hole exchange field. The Mn spins are (a) oriented initially along the $\hat{x}$ axis of the applied field, are (b) tipped into $\hat{y}$ by the transient hole exchange field, and (c) remain to precess about the applied field for long times.

B. Model for coherent rotation

The observation of Mn precession following optical pumping of spin-polarized excitons implies a mechanism involving the simultaneous ''tipping'' of a large number of Mn^{2+} spins all in the same direction. If the Mn spins were perturbed in random directions or if the tipping process occurred over time scales comparable to the Mn precession period, then no signal would be observed due to the arbitrary phases of the individual spins. The effect is not large—we calculate that if every Mn spin within the laser spot is equally affected, then the average tipping angle is of order 10 m deg at 1 T. There is no ''dc'' or long-lived spin-dependent offset to the signal—the Mn beats oscillate about exactly zero within the noise limits of the experiment. Moreover, it has been verified that an oppositely oriented circular pump results in a 180° phase shift of the Mn beats and that no long-lived signal is observed for a linear pump. We propose, then, that the mechanism lies in the coherent rotation of the Mn ensemble about the transient exchange field generated by the photoinjected hole spins. This model is illustrated schematically in Fig. 12 and proceeds as follows: (a) Before the arrival of the pump pulse, the Mn^{2+} spins are preferentially aligned along the $\hat{x}$ axis of the applied transverse field. (b) Immediately following photoexcitation, the electrons and holes are spin polarized along $\hat{z}$. The electron spins begin precessing, and the polarized hole spin population, which is constrained to lie along $\hat{z}$ by the effects of quantum confinement, generates an exchange field along $\hat{z}$, which decays exponentially with time. This exchange field exerts a torque on the Mn^{2+} spins, rotating the net Mn magnetization initially into the $\hat{y}$ axis. (c) At long times, after the holes and

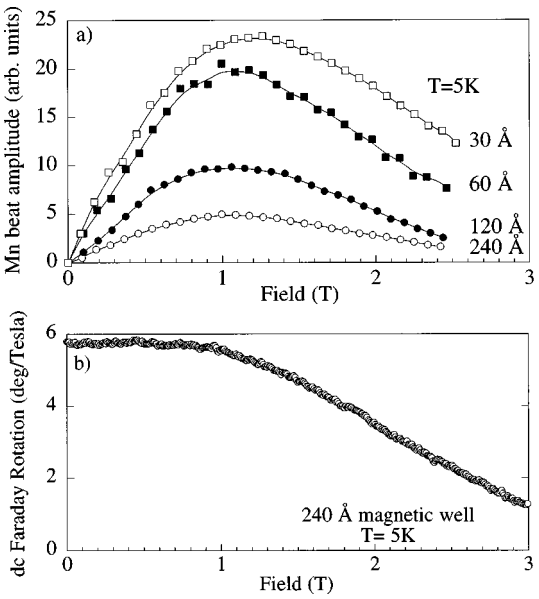

FIG. 13. (a) Normalized amplitude of the Mn beats vs applied transverse field for different well-width samples. (b) The Faraday response (Verdet constant or ''sensitivity'') of the 240-Å magnetic well to longitudinal fields as a function of applied transverse fields.

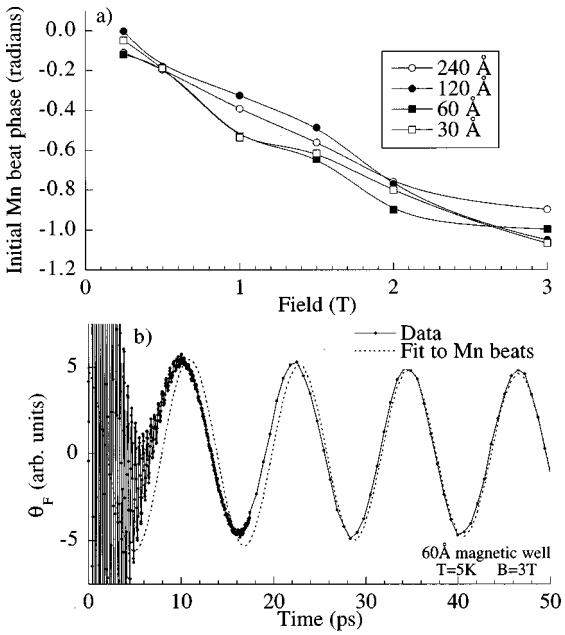

FIG. 14. (a) Intial phase of the Mn free-induction decay, as measured by fitting the Mn^{2+} beats to $Ae^{-t/\tau}\sin(\Omega_{Mn}t+\phi)$ and extrapolating back to zero time delay. (b) Dynamic phase shifting of the Mn^{2+} free-induction signal with respect to the fixed frequency of the fit. The phase shift at short times is due to the presence of ''invisible'' carriers which generate a demagnetizing field. The fit to the data is excellent for all times >35 ps.

electrons have recombined, the perturbed Mn magnetization remains to precess about the applied field, leading to small oscillations in the measured magnetization along $\hat{z}$. A very similar mechanism was invoked to account for the observation of up to 15 Mn spin-flip lines in the Raman spectra of magnetic quantum wells in transverse fields.[32] In effect, a single hole is tipping a large number of Mn spins within the spatial extent of its wave function. We do not consider the exchange field of the electron spin because of its weaker coupling to the Mn sublattice and its rapid oscillation which averages to zero.

This model of coherent rotation about the exchange field of the holes predicts several trends which are readily confirmed by experiment. The first prediction involves the measured amplitude of the Mn beats, which is expected to be proportional to the net sample magnetization and thus increase from zero with the applied field. This trend is indeed observed, as shown in Fig. 13(a) where the normalized amplitude of the Mn beats is measured as a function of applied field for all four magnetic samples at 5 K. In zero field there is no net magnetization and no Mn beats are observed. For a given sample, the amplitude of the Mn beats increases roughly linearly with applied field up to $\sim$1 T. In the absence of other effects, the amplitude of the Mn beats would eventually saturate, in keeping with the sample magnetization. The observed rolloff beyond 1 T in all the magnetic samples is due to the effect of the decreasing hole spin-relaxation time and also due to the fact that the samples' Verdet constants begin to decrease. The Verdet constant, a material parameter which characterizes the amount of Faraday rotation evoked per unit length and unit *field along* $\hat{z}$ (deg/cm T), is found in these samples to fall off in transverse fields greater than 1 T [Fig. 13(b)]. This is because the exciton absorption broadens and moves to lower energies, decreasing its spectral overlap with the laser (in effect, the measurement becomes less sensitive to a given oscillating sample magnetization along $\hat{z}$). Regardless, the linear increase in the Mn beat amplitude below 1 T is strong evidence in favor of the proposed model. In addition, this result rules out the possibility of polarization of the Mn sublattice by direct spin-flip scattering with the carriers, which would be expected to induce a long-lived magnetization along $\hat{z}$ even in zero field.

The normalized magnitude of the Mn oscillation signal is largest in the narrowest quantum well and decreases with increasing well width. This trend is consistent with a scenario of increased hole stability provided by the stronger quantum confinement in the narrower wells. The observed behavior is also qualitatively consistent with recent calculations that show a decrease in the number of Raman spin-flip resonances with increasing well width.[33] A longer-lived hole exchange field in narrower wells tips the Mn^{2+} moments further away from the axis of the applied field, leading to larger amplitude beats. Similarly, Raman studies have demonstrated an increased number of Mn spin-flip peaks in narrower wells.[32] However, as mentioned in Sec. IV C, we do not directly observe these implied longer hole spin lifetimes in the narrower quantum wells; all four magnetic quantum wells showed similar hole spin-relaxation times within experimental error. This discrepancy remains puzzling.

Last, because a rotation of the Mn^{2+} spins about the hole-exchange field initially tips the moments into the y axis, the Mn^{2+} precession signal should commence as a sinusoid. That is, if the Mn^{2+} beats are fit to an exponentially decaying sinusoid, $Ae^{-t/\tau}\sin(\Omega_{Mn}t+\phi)$, the oscillatory signal should extrapolate back to zero amplitude (or, alternatively, zero phase) at zero time delay. Figure 14(a) shows the initial phase of the Mn beats at 5 K as a function of applied field.

The data indicate that in the limit of small fields, the initial phase approaches zero. In fields, an extrapolation of the Mn beats back to zero time delay indicates that the Mn oscillation signal is initially positive, with negative slope. However, this effect is artificial. Careful analysis of the signal as compared to the fit at times near zero reveals an interesting phenomenon: The fit and the data develop an increasing phase shift as one looks ''backward'' in time towards zero delay, as shown in Fig. 14(b). Evidently, the Mn^{2+} spins initially begin precessing slowly and then accelerate to a higher frequency commensurate with $g=2.01$. The Mn^{2+} moments experience an initially reduced magnetic field which grows asymptotically to the applied magnetic field. This effect accounts for the nonzero initial phases shown in Fig. 14(a). We believe that during the $\sim$30 ps over which this effect is seen to occur the Mn^{2+} spins are experiencing the applied field *reduced by the demagnetization field of the spin-relaxed excitons*. Recall that the exciton recombination times are much longer than the spin lifetimes, and thus they are still present in the sample to $\sim$50 ps. The excitons have relaxed to their lowest-energy state and are preferentially oriented antiparallel to the applied field and are ostensibly invisible to the Faraday rotation probe. However, these oriented excitons generate a demagnetizing field in the sample, as was seen directly in Fig. 5(a) in the case of longitudinal fields. As the excitons recombine, the strength of the demagnetizing field decays to zero and the Mn spins precess faster about the ''bare'' applied field. Thus the presence of the ''invisible'' excitons is indirectly inferred through the precession frequency of the Mn moments, and we conclude that the measured Mn spins do indeed commence as a sinusoid, in support of the model for coherent rotation.

C. Electron paramagnetic resonance of the Mn spins

The decay time of the long-lived Mn^{2+} free-induction envelope should therefore be a measure of the Mn transverse spin-relaxation (dephasing) time, and indeed the times are in agreement with those measured using traditional electron-spin-resonance spectrometers in bulk samples with similar Mn concentration.[8] This allows for the exciting possibility of performing all-optical paramagnetic spin-resonance studies of the small numbers of Mn spins present in single quantum wells or heterostructures, where the reduced dimensionality directly affects formation of frustrated and ordered magnetic phases.[34,35]

It is relevant to briefly review the essential findings of earlier EPR studies in bulk diluted magnetic semiconductors so as to compare these with the time-domain EPR measurements in the present samples. Extensive studies of EPR in the bulk magnetic semiconductor alloys have revealed that the linewidths, which are Lorentzian at high temperatures, broaden with either increasing Mn concentration or decreasing temperature.[36–39] The high-temperature values of the observed linewidths can be understood within the framework of exchange narrowing models which consider the effects of the strong isotropic and weak anisotropic contributions to the superexchange between nearest-neighbor Mn moments.[36,40] The broadening of the EPR linewidth with decreasing temperature has been attributed to two contributions that arise within the Mori-Kawasaki formalism of exchange narrowing: (a) The linewidth is inversely proportional to $(T\chi_0)$, where χ_0 is the Curie-Weiss static magnetic susceptibility, and (b) the linewidth is proportional to a function involving dynamic spin-spin correlations. The former accounts for the temperature dependence at higher temperatures, while the latter becomes important at low temperatures on approaching a spin glass transition. At the lowest temperatures studied ($1.5\ \mathrm{K}<T<\sim 20\ \mathrm{K}$) and high Mn concentrations, the EPR line shapes deviate significantly from Lorentzian behavior and shift to lower fields. Despite detailed efforts to account for this effect within the context of a variable g factor or using an internal magnetic field along some preferred direction, there is no satisfactory explanation for this behavior. It is precisely within this regime of low temperatures and high Mn concentrations that spin-spin correlations between Mn^{2+} moments dominate and lead to freezing of spins in bulk samples; unfortunately, analysis of EPR line shapes in this low-temperature, high-concentration limit becomes difficult both because of the large linewidths [full width at half maximum (FWHM) >2 T] and the absence of a theory for the non-Lorentzian line shapes. Our expectation is that an all-optical technique providing true time-domain data (rather than spectral data) on the spin resonance of strongly spin-correlated Mn moments can illuminate the interactions involved, especially within specifically engineered magnetic environments possible with MBE-grown heterostructures. Growth of dilute magnetic semiconductor heterostructures results in three-dimensional distributions of Mn spins, and the crossover to two-dimensional spin distributions can be realized with ''digital'' growth.

The time resolution of the optical method is well suited to study the very fast Mn dephasing times that occur at low temperatures. Moreover, this optical scheme works equally well over a wide range of applied magnetic fields (0.25–6 T in the present experiments), permitting frequency-dependent spin-resonance studies of the Mn^{2+} moments from $\sim$7 to 170 GHz. Tunability of the microwave frequency can be difficult to realize in traditional high-frequency EPR spectrometers where the frequency scale is set by the geometry of the resonant cavity. Using this optical technique, spin-resonance studies of 2D spin distributions of MnSe were recently conducted,[8] where it was found that as the fractional monolayer coverage of individual MnSe planes was increased from roughly 10% to unity, the Mn spin dephasing rate increased dramatically, indicating the strong short-range spin-spin interactions between the Mn^{2+} moments. Also, temperature-dependent studies revealed longer dephasing lifetimes at elevated temperatures, in agreement with the narrowing linewidths measured in bulk systems with traditional EPR methods. Exploiting the field tunability of the optical technique, it was observed that the field dependence of the dephasing rate was relatively weak in the case of low local Mn density, but very strong in the case of high concentration.[8]

In no case do the time-resolved data show evidence of a variable manganese g factor, even in samples with very high local Mn density at low temperatures. However, the free-induction decay of the Mn^{2+} ions develops a markedly non-exponential behavior. Figure 15(a) shows one such free-induction decay, taken at 5 K and 1 T (28 GHz) in a digital sample with discrete full monolayer planes of MnSe. In this

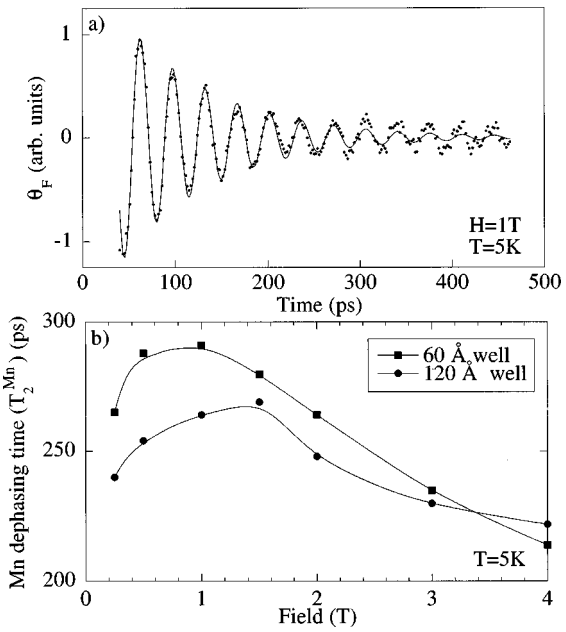

FIG. 15. (a) Nonexponential Mn^{2+} free-induction decay in a sample with very high local density of Mn^{2+} ions. The data deviate considerably from the smooth line, which is an exponentially decaying best fit. (b) The measured manganese transverse spin-relaxation time as a function of field in the 60- and 120-Å magnetic quantum wells. Lines are guides to the eye.

sample, the local Mn density is very high, of the order of 50%, accounting for interdiffusion during growth. The free-induction signal is seen to decay initially rapidly, followed by a slower decay. This behavior is made more clear by noting the disparity at long time delays between the data and the smooth line in the Fig. 15(a), which is a single exponentially decaying best fit to the data. A Fourier transform of this data does indeed result in a non-Lorentzian spectral line shape, but does not exhibit a shift in the resonance peak.

In the present series of magnetic wells, the transverse spin relaxation or dephasing time (T_2^{Mn}) of the Mn^{2+} spins occurs on a time scale of roughly 275 ps at 1 T (28 GHz) for all four well widths. The four wells possess nominally identical microscopic densities of Mn spins (quarter-monolayer planes of MnSe), and so only small differences in T_2^{Mn} between the wells is measured. Characteristic field-dependent Mn dephasing times in these samples are given in Fig. 15(b) and show a marked field dependence to T_2^{Mn}. At high fields, T_2^{Mn} decreases as the interacting Mn spin dephase more rapidly. However, our data show that at the lowest fields T_2^{Mn} is also found to accelerate, giving a broad peak in the measured dephasing time at $\sim$1 T.

VI. CONCLUSION

In summary, we have described an all-optical technique suited to ultrafast time-domain spin-resonance studies in magnetic semiconductor heterostructures. This pump-probe Faraday rotation experiment reveals the spin dynamics of excitons in zero field and in longitudinal applied magnetic fields. In transverse magnetic fields (Voigt geometry), the oscillatory free-induction decays of photoinjected electron spins can be measured with excellent signal to noise, providing a direct measure of the electron intraband coherence time (spin-relaxation time) distinct from the spin relaxation of the holes. Measurements in a series of magnetic quantum wells of different widths reveal terahertz Larmor precession of the electron spins, indicating amplified electron g factors ranging from $g^e = 38.3$ in the narrowest 30-Å well to $g^e = 75.8$ in the widest 240-Å well. Moreover, comparison with the exciton Zeeman splitting in longitudinal magnetic fields yields precise measurement of the hole g factors. The electron and hole g factors decrease in concert with decreasing well width, in accordance with their calculated overlap with the magnetic planes.

Based on present and previously published data, we empirically distinguish between weakly and strongly coupled magnetic quantum wells. In the former case, the carrier wave functions have only a limited overlap with the magnetic Mn ions, possibly due to intrinsic disorder which can localize the carriers. Such samples exhibit broad absorption linewidths, small effective g factors, and longer spin- and phase-relaxation times. In contrast, strongly coupled magnetic samples exhibit large effective g factors, suggesting higher-quality samples (narrow linewidths) containing delocalized carriers with a large wave function overlap with the local magnetic moments. However, this strong interaction with the magnetic moments can lead to rapid spin and phase relaxation of the photoinjected carriers.

Electron and hole spin-relaxation times in magnetic quantum wells are found to be much more rapid than in their nonmagnetic counterparts, suggesting the role of the local Mn moments in dominating the measured carrier spin relaxation through carrier-ion spin-flip interactions. With increasing photoinjected carrier density in magnetic quantum wells, the electron spin-relaxation time τ_e is observed to increase in conjunction with a decreased Larmor frequency. At elevated temperatures (up to 130 K, τ_e remains unchanged in magnetic quantum wells, while increasing dramatically above $\sim$70 K in nonmagnetic strucutres. With applied field, τ_e in nonmagnetic and weakly magnetic wells shows a marked minimum at fields of 2–3 T, which we tentatively ascribe to the situation in which the electron Zeeman energy overcomes electron-hole exchange energy ($\sim$250 μeV). In strongly coupled magnetic wells, τ_e is much less and shows only slight field dependence, reflecting the dominance of the electron–Mn-ion scattering interaction over other, less efficient scattering mechanisms.

Measurements of hole dynamics suggests that the hole spin-relaxation times (τ_h) are governed by mixing between the hole bands, which in turn is determined by the competition between the confinement potential (hh-lh splitting) and the Zeeman energy. In nonmagnetic quantum wells the field-dependent hole spin-relaxation time is minimally affected, because the Zeeman energy remains much less than the hh-lh splitting and the hole bands remain unmixed. In contrast, the Zeeman energy in magnetic quantum wells rapidly dominates the hh-lh splitting in modest applied fields and τ_h decreases dramatically with applied field as the hole bands mix and the hole spins reorient from the growth axis to the axis of the applied field. Against expectation, we did not observe significant variation in τ_h for the different well-width samples.

Free-induction decays of Mn ions are induced by the co-

herent rotation of the Mn sublattice about the transient exchange field of the photoexcited holes. The Mn beat amplitude is linear with small applied fields, and the beats commence sinusoidally, in support of the proposed model for coherent rotation. The Mn beat signal increases with decreasing well width, providing indirect evidence that the hole spin acquires additional stability against scattering with increasing quantum confinement. In direct analogy with EPR experiments, the Mn free-induction decay provides a measure of T_2^{Mn}, the transverse spin-relaxation time. This all-optical method of time-domain EPR enables the study of monolayer and fractional-monolayer magnetic planes, and the femtosecond time resolution is especially suited to the regime of low temperatures and high magnetic concentrations, where T_2^{Mn} is very fast. Moreover, this method facilitates field-dependent EPR, and in the present series of magnetic quantum wells containing quarter-monolayer planes of MnSe, T_2^{Mn} is measured at frequencies of 7–170 GHz (0.25–6 T) and is found to be markedly field dependent. We anticipate that the optical spin-resonance methods described in this paper will aid in the understanding of carrier spin relaxation in magnetic semicondctor heterostructures and also elucidate the resonance behavior of paramagentic ions in quantum confined geometries.

ACKNOWLEDGMENTS

This work was supported by Grant Nos. NSF DMR-92-07567, NSF DMR-95-00460, AFOSR F49620-96-1-0118, and the QUEST NSF Science and Technology Center DMR 91-20007.

[1] D. S. Chemla, Phys. Today **46**(6), 46 (1993).
[2] A. Vinattieri *et al.*, Phys. Rev. B **50**, 10 868 (1994).
[3] J. Shah *et al.*, Surf. Sci. **267**, 304 (1992).
[4] S. Bar-Ad and I. Bar-Joseph, Phys. Rev. Lett. **68**, 349 (1992).
[5] J. J. Baumberg *et al.*, Phys. Rev. B **50**, 7689 (1994).
[6] S. T. Cundiff *et al.*, J. Opt. Soc. Am. B **13**, 1263 (1996).
[7] S. A. Crooker *et al.*, Phys. Rev. Lett. **75**, 505 (1995).
[8] S. A. Crooker *et al.*, Phys. Rev. Lett. **77**, 2814 (1996).
[9] S. A. Crooker, D. D. Awschalom, and N. Samarth, IEEE J. Sel. Top. Quantum Electron. **1**, 1082 (1995).
[10] J. K. Furdyna and N. Samarth, J. Appl. Phys. **61**, 3526 (1987).
[11] I. Smorchkova and N. Samarth, Appl. Phys. Lett. **69**, 1640 (1996).
[12] G. Bastard, *Wave Mechanics Applied to Semiconductor Heterostructures* (Halstead Press, New York, 1988).
[13] R. W. Martin *et al.*, Phys. Rev. B **42**, 9237 (1990).
[14] P. Peyla *et al.*, Phys. Rev. B **47**, 3783 (1993).
[15] B. Kuhn-Heinrich *et al.*, Solid State Commun. **91**, 413 (1994).
[16] B. Kuhn-Heinrich and W. Ossau, Mater. Sci. Forum **182**, 491 (1996).
[17] W. Y. Yu *et al.*, Phys. Rev. B **51**, 9722 (1995).
[18] M. Z. Maialle, E. A. d. A. e. Silva, and L. J. Sham, Phys. Rev. B **47**, 15 776 (1993).
[19] A. Vinattieri *et al.*, Solid State Commun. **88**, 189 (1993).
[20] T. C. Damen *et al.*, Appl. Phys. Lett. **58**, 1902 (1991).
[21] S. Bar-Ad and I. Bar-Joseph, Phys. Rev. Lett. **66**, 2491 (1991).
[22] A. J. Fischer *et al.*, Phys. Rev. B **50**, 17 643 (1994).
[23] R. E. Worsley *et al.*, Phys. Rev. Lett. **76**, 3224 (1996).
[24] J. J. Baumberg *et al.*, Phys. Rev. Lett. **72**, 717 (1994).
[25] S. A. Crooker, D. D. Awschalom, and N. Samarth (unpublished).
[26] J. B. Stark, W. H. Knox, and D. S. Chemla, Phys. Rev. B **46**, 7919 (1992).
[27] T. C. Damen *et al.*, Phys. Rev. Lett. **67**, 3432 (1991).
[28] D. D. Awschalom *et al.*, Phys. Rev. Lett. **66**, 1212 (1991).
[29] H. Krenn *et al.*, Phys. Rev. B **39**, 10 918 (1989).
[30] A. P. Heberle, W. W. Ruhle, and K. Ploog, Phys. Rev. Lett. **72**, 3887 (1994).
[31] M. Oestreich *et al.*, Phys. Rev. B **53**, 7911 (1996).
[32] J. Stuhler *et al.*, Phys. Rev. Lett. **74**, 2567 (1995).
[33] K. V. Kavokin and I. A. Merkulov, Phys. Rev. B **55**, 7371 (1997).
[34] N. Samarth *et al.*, Phys. Rev. B **44**, 4701 (1991).
[35] D. D. Awschalom *et al.*, Phys. Rev. Lett. **59**, 1733 (1987).
[36] N. Samarth and J. K. Furdyna, Phys. Rev. B **37**, 9227 (1988).
[37] R. E. Kremer and J. K. Furdyna, Phys. Rev. B **32**, 5591 (1985).
[38] S. B. Oseroff and P. H. Keesom, in *Diluted Magnetic Semiconductors*, edited by J. K. Furdyna and J. Kossut (Academic, San Diego, CA, 1988), p. 73.
[39] H. A. Sayad and S. M. Bhagat, Phys. Rev. B **31**, 591 (1985).
[40] B. E. Larson and H. Ehrenreich, Phys. Rev. B **39**, 1747 (1989).